



Nanocomposite Counter Electrode Materials for Electrochromic Windows

Dane Gillaspie,^{a,*} Andrew Norman,^a C. Edwin Tracy,^a J. Roland Pitts,^a
Se-Hee Lee,^{b,*} and Anne Dillon^{a,*}

^aNational Renewable Energy Laboratory, Golden, Colorado 80401, USA

^bDepartment of Mechanical Engineering, University of Colorado, Boulder, Colorado 80309, USA

Nickel-oxide-based nanocomposite films were deposited using radio-frequency magnetron sputtering from ceramic targets composed of lithium, nickel, and tungsten oxides. The resulting films are partially prelithiated and exhibit a slight spectral shift relative to tungsten-free films when colored. Electron microscopy and X-ray diffraction show that the films are composed of nanocrystallites with NiO structure. The films show promise as electrochromic counter electrode layers that are durable, efficient, and fabricated using a scalable, economical process.

© 2010 The Electrochemical Society. [DOI: 10.1149/1.3276779] All rights reserved.

Manuscript submitted August 26, 2009; revised manuscript received November 23, 2009. Published January 20, 2010.

The electrochromic (EC) effect, which occurs for many transition-metal oxide materials, and the possible use of EC materials in devices were widely publicized by Deb in 1969.¹ Electrochromism may be defined as transmittance modulation that occurs reversibly by electrically controlling the oxidation states of the transition metal. “Smart” windows, which employ EC films, offer substantial energy savings as well as increased comfort for building occupants.^{2,3} In addition to building windows, EC devices are also used in vehicles for moonroofs and rearview mirrors.

As with nearly all renewable energy technologies, there is a strong demand for high performance materials that are also cost-effective. In EC materials, this requires the use of standard industrial production techniques to produce films with high coloration efficiency (CE), rapid switching speed, and robust reversibility. Furthermore, EC “smart window” devices must be able to withstand cycling multiple times per day for decades, even when they are exposed to harsh conditions with extreme temperatures and intense UV radiation.

EC properties in metal oxides occur with the simultaneous intercalation of positive ions and charge-compensating electrons. Materials can either darken cathodically with the insertion of positive ions, as can WO₃ and MoO₃, or they can color anodically with the removal of positive ions after insertion, as can NiO, CoO, and Ir₂O₃.^{4,5} Although it is possible to construct a complete solid-state device with only a single coloring layer, it is preferable to build a complementary device with two matched coloring layers, one anodic and one cathodic. Both active layers would then become darker as the charge-compensating ion, Li⁺ or H⁺, is moved from the anodic counter electrode to the cathodic working electrode, and both layers would become transparent as the process is reversed. By combining an electrode that exhibits cathodic coloration with a counter electrode that has an anodic coloration, it is possible to fabricate a more efficient and visually appealing EC device.

The conventional cathodic layer, WO₃, is widely known and has had a long developmental history. Substoichiometric WO₃ films have the highest CE over the visible region, fast response times, and long lifetimes.⁶⁻⁸ Tungsten oxides are therefore the most widely employed in industry, as evidenced by the characteristic blue tint in most commercial devices. However, a definitive choice for the counter electrode material remains less clear.⁵ Nickel oxide and its derivatives are a common choice, but there are ongoing concerns with both durability and performance.⁸⁻¹¹

In this paper, we describe our development of a counter electrode material that shows promise in terms of both durability and performance and is grown using common vacuum deposition methods and

materials. The counter electrode films are formed by sputter deposition from a composite ceramic lithium, nickel, and tungsten oxide target. Consistent with previous reports, NiO nanocrystallites are observed to form.^{12,13} Secondary phases from the other elements present in the sample are not observed, which implies that they act as substitutional or interstitial dopants or segregate to the grain boundaries and form an amorphous layer between the NiO crystallites.

Experimental

Radio-frequency (rf) magnetron sputtering was used to deposit the nanocomposite films from ceramic targets. Magnetron sputtering is a very common deposition technique to deposit coatings on glass, and it allows a great deal of flexibility in material choice. Targets were produced using Li₂CO₃, NiO, and WO₃ powders. The powders were mixed, pressed, and calcined at 700°C to remove CO₂ and were then ground, pressed, and sintered twice to produce dense 2 in. ceramic sputtering targets. The weight of the target material after each step was consistent with the retention of the Li:Ni:W ratio. RF sputtering was used due to the low conductivity of the target. The standard deposition gas mixture was Ar:O₂ = 1:1 with a total deposition pressure of 10 mTorr and a deposition power of 50 W. Substrate temperature during deposition was not controlled, but the substrate was mounted to a very large 125 cm diameter aluminum plate, with a thickness of 2 cm, and the back-side temperature did not exceed 50°C. The film surface temperature was significantly higher due to the heating mechanisms inherent in rf sputtering. The target-substrate distance was 10 cm, and the base pressure for the chamber was below 1 × 10⁻⁶ Torr.

The resulting films were characterized using transmission electron microscopy (TEM), X-ray diffraction (XRD), optical transmission, and reflection spectroscopy, as well as electrochemical measurements. TEM was performed in an FEI F20 UltraTwin operated at 200 kV and in a Philips CM30 operated at 300 kV. The XRD data were taken with a two-dimensional detector. The broad amorphous diffraction from the glass substrate was subtracted from the two-dimensional data set, so that the relatively weak diffraction peaks from the nanocrystalline film are more evident. Electrochemical and EC properties were measured in a liquid electrolyte half-cell (1 M LiClO₄-PC, where PC is propylene carbonate) with a lithium counter/reference electrode.

Results and Discussion

Figure 1a shows a low resolution TEM bright-field image of a half-cell device formed by rf sputtering of the composite target on fluorine-doped tin oxide-coated glass (Pilkington Tec 15). The resulting nanocomposite film is flat and featureless at this length scale, with no visible porosity or significant defects. This lack of porosity is consistent with a high effective growth temperature.¹⁴ The

* Electrochemical Society Active Member.

^z E-mail: dane.gillaspie@nrel.gov

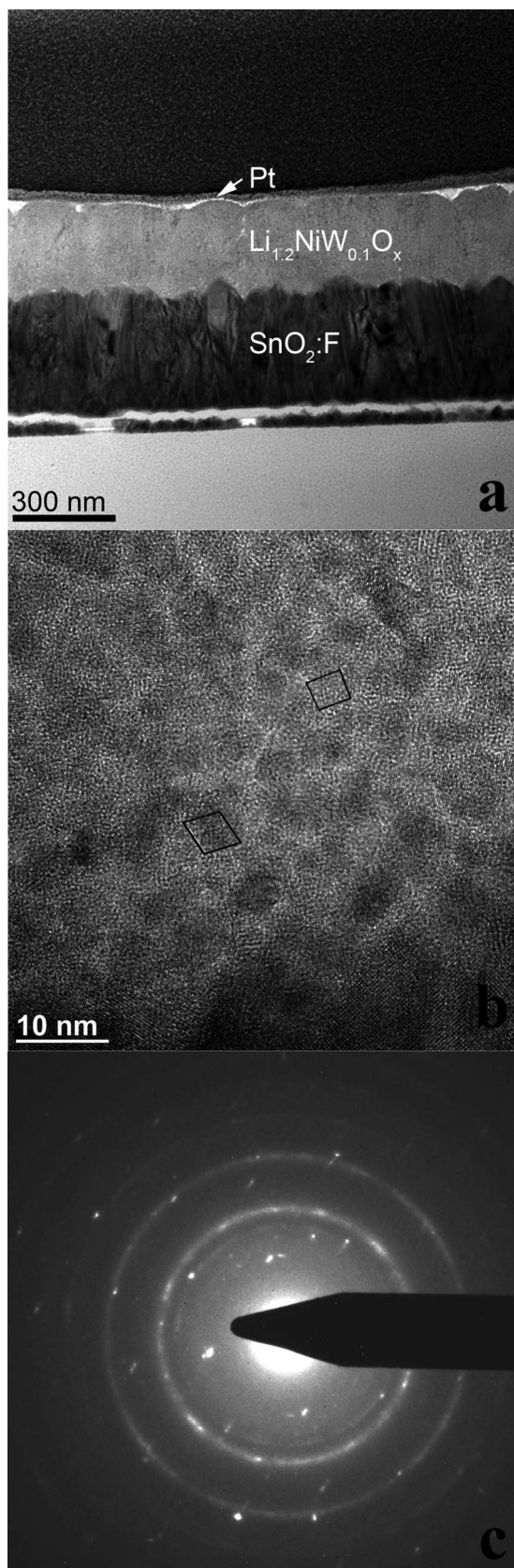


Figure 1. TEM results for $\text{Li}_{1.2}\text{NiW}_{0.1}\text{O}_x$ composite film. (a) Low resolution TEM image of $\text{Li}_{1.2}\text{NiW}_{0.1}\text{O}_x$ composite film on fluorine-doped tin oxide substrate. (b) High resolution TEM image of the $\text{Li}_{1.2}\text{NiW}_{0.1}\text{O}_x$ composite film, with two crystallites highlighted in black. (c) Selected-area electron diffraction from $\text{Li}_{1.2}\text{NiW}_{0.1}\text{O}_x$ composite film.

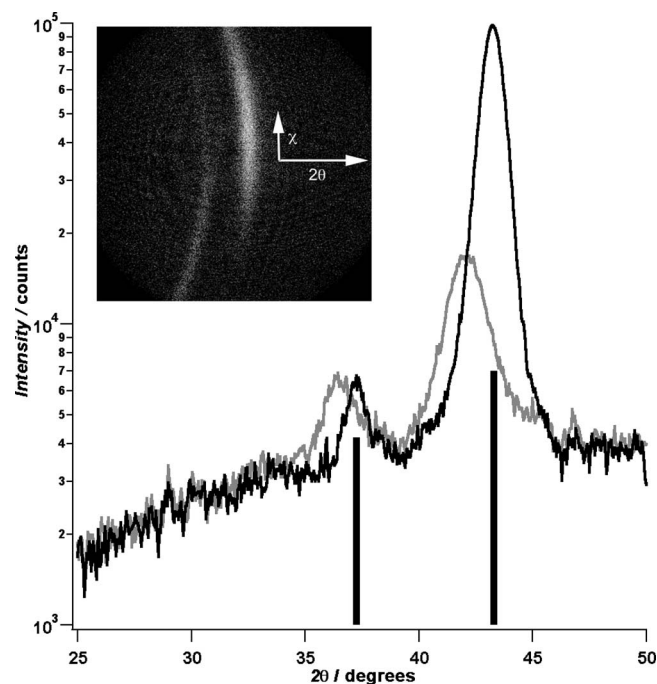


Figure 2. XRD patterns from $\text{Li}_{1.2}\text{NiW}_{0.1}\text{O}_x$ composite films prepared on glass substrates. Light gray pattern is from as-deposited sample, and dark gray pattern is from sample annealed at 438°C . Inset shows raw two-dimensional detector data for annealed film with 2θ and χ directions indicated.

fluorine-doped tin oxide conducting layer has large crystallites that lead to some small corrugation in the surface of the nanocomposite film. The platinum layer was applied to protect the sample surface during cross-sectional sample preparation in an FEI Nova 200 focused-ion-beam workstation. Figure 1b is a high resolution image of the nanocrystalline structure of the film. The size of the crystallites is 5–10 nm, with lattice fringes clearly evident throughout. Two of the crystallites are outlined in black. Figure 1c shows the selected-area electron diffraction pattern taken from a film deposited under similar conditions. The spacing of the diffraction rings is consistent with the rhombohedral NiO structure (JCPDS no. 44-1159). A diffraction spot pattern that may be attributed to the fluorine-doped tin oxide substrate is also apparent.

This NiO structure was confirmed by XRD. Figure 2 shows the diffraction patterns from two pieces of a film grown from a $\text{Li}_{1.2}\text{NiW}_{0.1}\text{O}_x$ composite target using Corning Eagle 2000 borosilicate glass as the substrate. The lower intensity pattern (gray) was measured from the as-grown film. The inset shows the raw two-dimensional detector diffraction data from the Bruker D8 diffractometer. To help confirm the NiO structure and check for thermal stability, a brief annealing experiment was performed. The second, more intense pattern (black) was measured after annealing a second piece of the same film in argon for 1 h at 438°C . The broadness of the initial peaks is consistent with the 5–10 nm size distribution obtained from TEM imaging. A Debye–Scherrer analysis of the narrowing of the diffraction lines after annealing implies that the crystallites have doubled in diameter with the heat-treatment. The as-grown film peaks are shifted relative to the annealed peaks, with the [101] peak shifted by $0.86 \pm 0.03^\circ$ and the [012] peak shifted by $1.16 \pm 0.03^\circ$. The measured angular range is too small for a detailed Rietveld analysis, but the shift in the two peaks is consistent with an expansion of the unit cell volume of more than 8% in the as-deposited films.

The as-grown film exhibits an intermediate coloration between the dark (oxidized) and light (bleached) states, indicating that there has been a partial intercalation of lithium during film growth. According to previous work on sputtered lithium–nickel oxide com-

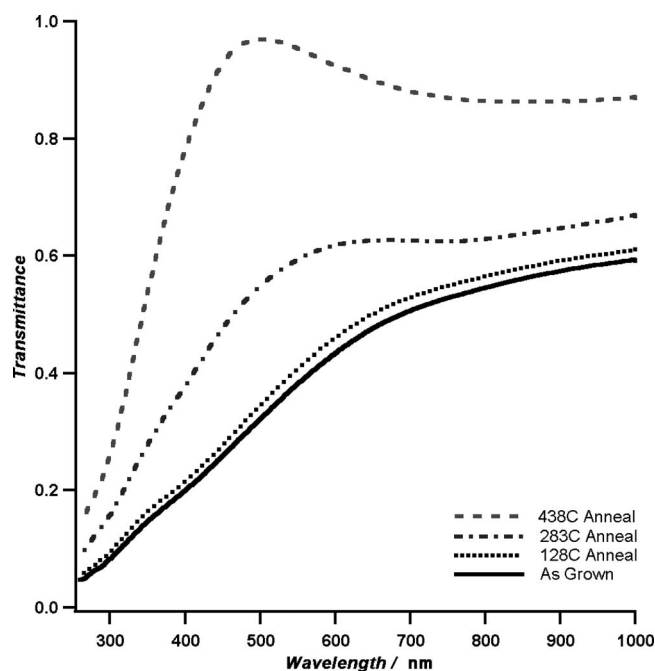


Figure 3. Transmittance data from as-grown and annealed $\text{Li}_{1.2}\text{NiW}_{0.1}\text{O}_x$ composite films prepared on glass substrates.

pounds,^{15,16} this is consistent with the formation of $\text{Li}_x\text{Ni}_{1-x}\text{O}$ crystallites. As the film is annealed, the film bleaches strongly (Fig. 3) as the average lattice parameters revert to bulk NiO values (Fig. 2). Because the amount of lithium in the film presumably does not change drastically at this temperature and time scale, there is a reduction of the film due to oxygen loss at the grain boundaries. The opposite effect is seen in nickel oxide films exposed to ozone.¹⁷

Figure 4 shows the in situ transmittance at 670 nm and cyclic voltammogram (CV) for a 100 nm thick $\times 1 \text{ cm}^2$ $\text{Li}_{1.2}\text{NiW}_{0.1}\text{O}_x$

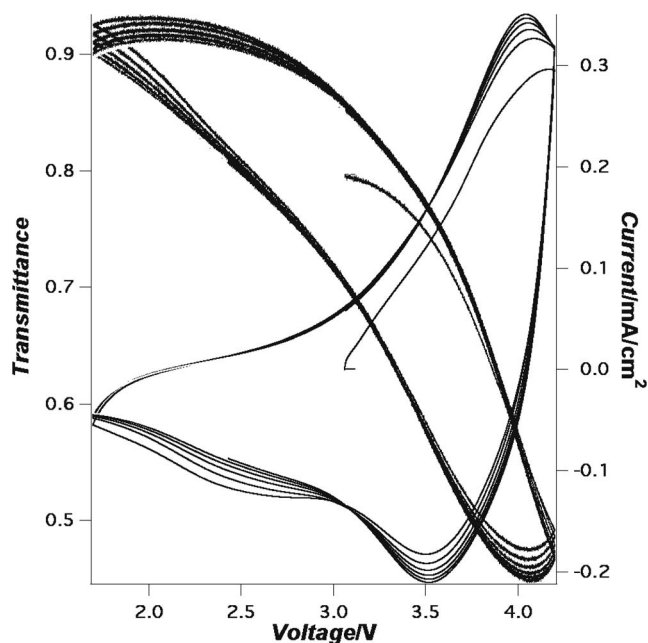


Figure 4. CV and in situ transmittance for 100 nm $\times 1 \text{ cm}^2$ composite film grown from a $\text{Li}_{1.2}\text{NiW}_{0.1}\text{O}_x$ target on $\text{SnO}_2\text{:F}$ -coated substrate. The lightness of the traces increases with cycle number, so that trends can be seen more easily.

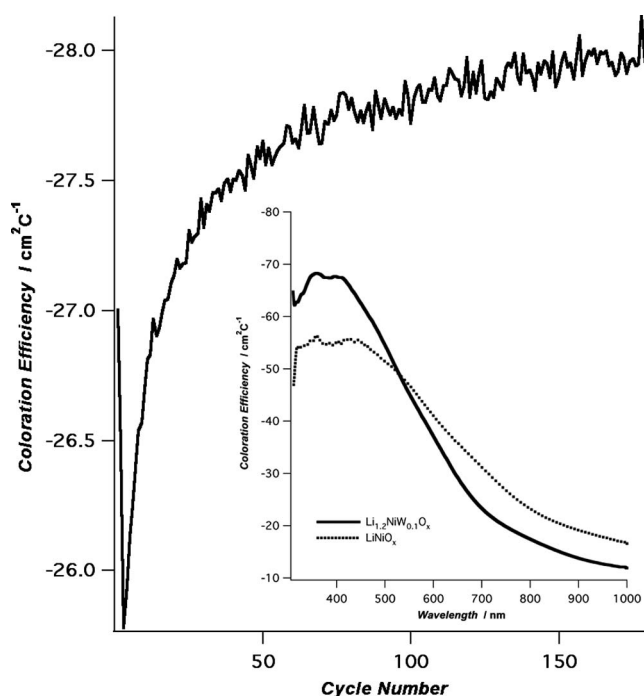


Figure 5. CE vs cycle number for $\text{Li}_{1.2}\text{NiW}_{0.1}\text{O}_x$ composite films cycled in liquid electrolyte. Inset figure shows the CE vs wavelength for an equivalent film cycled in liquid electrolyte measured ex situ. Data for a LiNiO_x composite film prepared under similar conditions are shown for comparison.

composite film cycled at 10 mV/s in the half-cell configuration vs lithium. Due to the short residence time at high and low voltages, the transmittance window is somewhat smaller than that shown for the same film in Fig. 6. The shape of the CV is quite similar to that published for NiO films containing W^{11,18} and V¹⁹ cycled in non-aqueous electrolytes vs lithium. The magnitude of the insertion and removal current peaks at 3.5 and 4.0 V increases during the first few cycles, while the broad secondary peak at 2.5 V fades quickly. This implies that it corresponds to an irreversible side reaction. There is a small inflection in the transmittance curve at this voltage, meaning that the side reaction likely interferes with the main bleaching process.

One of the primary figures of merit for EC materials is CE. CE, $\eta(\lambda)$, is the change in optical density per unit charge per unit area. For films where the change in reflectance is small, this is often approximated by

$$\eta(\lambda) = \frac{\ln\left(\frac{T_{\text{bleached}}}{T_{\text{colored}}}\right)}{Q/A} \quad [1]$$

Figure 5 shows the evolution of the CE at 670 nm measured in situ for a 90 nm thick film grown using a $\text{Li}_{1.2}\text{NiW}_{0.1}\text{O}_x$ target cycled under constant current conditions in 1 M $\text{LiClO}_4\text{-PC}$. The CE decreases for the first several cycles, due to irreversible lithium loss in noncoloring processes. It is believed that these are primarily related to solid electrolyte interface formation and reactions near the surface, which is consistent with the recent work on LiNiO_2 cathode materials.^{20,21} These processes continue through the end of the cycling study, but as they decrease in magnitude, the CE converges to a value of 28 cm^2/C . This is consistent with those previously quoted.^{11,22,23} We note that the CE of 28 cm^2 is also stable over 180 cycles. The inset in Fig. 5 shows the CE as a function of wavelength, calculated from ex situ transmission measurements. The dark line is for the $\text{Li}_{1.2}\text{NiW}_{0.1}\text{O}_x$ composite, with the dashed line for a LiNiO_x film of equivalent thickness grown under similar conditions from a target prepared in the same manner as the $\text{Li}_{1.2}\text{NiW}_{0.1}\text{O}_x$

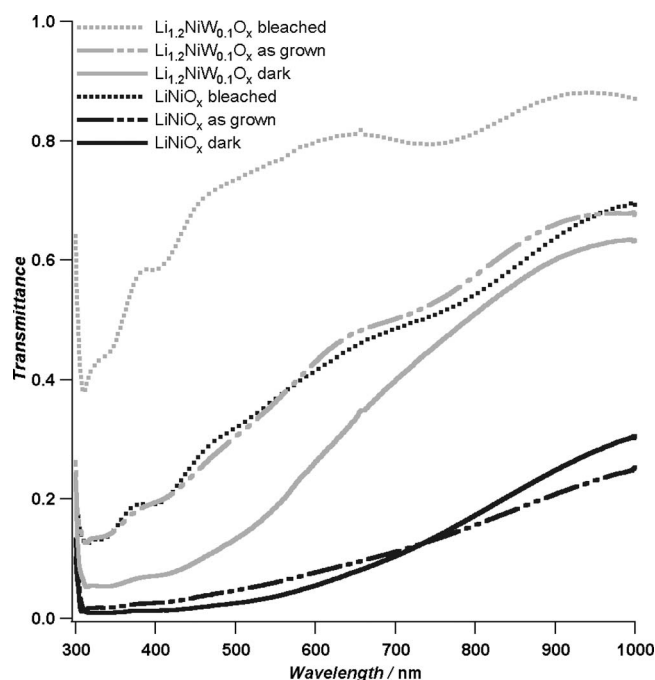


Figure 6. Ex situ transmittance scans for $\text{Li}_{1.2}\text{NiW}_{0.1}\text{O}_x$ and LiNiO_x films. Solid lines indicate dark-state measurements, dashed lines indicate bleached-state measurements, and mixed lines indicate as-grown measurements.

composite film target without tungsten. The CE peak is shifted toward shorter wavelengths for the W-doped film, which is consistent with changes observed by Avendaño et al. for doped NiO films cycled in aqueous electrolytes.²⁴ The transmittance data for both the $\text{Li}_{1.2}\text{NiW}_{0.1}\text{O}_x$ (dashed) and LiNiO_x (solid) films are shown in Fig. 6. Even though the thicknesses and stoichiometries are similar, both the bleached and dark states are more transparent for the $\text{Li}_{1.2}\text{NiW}_{0.1}\text{O}_x$ nanocomposite film.

Conclusions

EC thin films were grown using rf sputtering from composite ceramic targets containing lithium, nickel, and tungsten oxides. The resulting films are nanocrystalline with a NiO structure, and they show strong, repeatable color change when cycled. The peak CE of the film is blueshifted for the nanocomposite film compared to pure lithium–nickel oxide films. The CE shows no signs of degradation over 180 cycles. The bleached state of the $\text{Li}_{1.2}\text{NiW}_{0.1}\text{O}_x$ nanocomposite film is significantly more transparent than that of a similarly prepared LiNiO_x film. This can be advantageous in device fabrica-

tion because it allows for the film to be charge-balanced with a thicker WO_3 electrode to produce a larger coloration range.

Acknowledgments

This work was supported by the U.S. Department of Energy under contract no. DE-AC36-08-GO28308 with the National Renewable Energy Laboratory as part of the DOE Office of Energy Efficiency and Renewable Energy Office of Building Technologies program. The authors also thank Kim Jones for the focused-ion-beam sample preparation.

National Renewable Energy Laboratory assisted in meeting the publication costs of this article.

References

1. S. K. Deb, *Appl. Opt.*, **8**, 192 (1969).
2. D. Arasteh, S. Selkowitz, J. Apte, and M. LaFrance, in *Proceedings of the ACEEE Summer Study on Energy Efficiency in Buildings*, Lawrence Berkeley National Laboratory (2006).
3. B. Griffith, N. Long, P. Torcellini, R. Judkoff, D. Crawley, and J. Ryan, Report no. NREL/TP-550-41957, National Renewable Energy Laboratory (2007).
4. C. G. Granqvist, *Handbook of Inorganic Electrochromic Materials*, Elsevier, New York (1995).
5. P. Monk, R. Mortimer, and D. Rosseinsky, *Electrochromism and Electrochromic Devices*, Cambridge University Press, Cambridge, U.K. (2007).
6. C. Bechinger, M. S. Burdis, and J. G. Zhang, *Solid State Commun.*, **101**, 753 (1997).
7. S.-H. Lee, H. M. Cheong, J.-G. Zhang, A. Mascarenhas, D. K. Benson, and S. K. Deb, *Appl. Phys. Lett.*, **74**, 242 (1999).
8. J. Smulko, A. Azens, R. Marsal, L. B. Kish, S. Green, and C. G. Granqvist, *Sol. Energy Mater. Sol. Cells*, **92**, 914 (2008).
9. I. Bouessay, A. Rougier, P. Poizot, J. Moscovici, A. Michalowicz, and J. M. Tarascon, *Electrochim. Acta*, **50**, 3737 (2005).
10. N. Penin, A. Rougier, L. Laffont, P. Poizot, and J. M. Tarascon, *Sol. Energy Mater. Sol. Cells*, **90**, 422 (2006).
11. S.-H. Lee, Y.-S. Park, and S.-K. Joo, *Solid State Ionics*, **109**, 303 (1998).
12. X. F. Chen, X. F. Hu, and J. W. Feng, *Nanostruct. Mater.*, **6**, 309 (1995).
13. D. A. Wruck and M. Rubin, *J. Electrochem. Soc.*, **140**, 1097 (1993).
14. W. D. Westwood, *Sputter Deposition*, p. 285, AVS, New York (2003).
15. F. Michalak, K. von Rottkay, T. Richardson, J. Slack, and M. Rubin, *Electrochim. Acta*, **44**, 3085 (1999).
16. M. Rubin, S. J. Wen, T. Richardson, J. Kerr, K. von Rottkay, and J. Slack, *Sol. Energy Mater. Sol. Cells*, **54**, 59 (1998).
17. A. Azens, G. Gustavsson, R. Karmhag, and C. G. Granqvist, *Solid State Ionics*, **165**, 1 (2003).
18. S. H. Lee, H. M. Cheong, N. G. Park, C. E. Tracy, A. Mascarenhas, D. K. Benson, and S. K. Deb, *Solid State Ionics*, **140**, 135 (2001).
19. F. Artuso, F. Bonino, F. Decker, A. Lourenco, and E. Masetti, *Electrochim. Acta*, **47**, 2231 (2002).
20. S. Muto, Y. Sasano, K. Tatsumi, T. Sasaki, K. Horibuchi, Y. Takeuchi, and Y. Ukyo, *J. Electrochem. Soc.*, **156**, A371 (2009).
21. T. Sasaki, T. Nonaka, H. Oka, C. Okuda, Y. Itou, Y. Kondo, Y. Takeuchi, Y. Ukyo, K. Tatsumi, and S. Muto, *J. Electrochem. Soc.*, **156**, A289 (2009).
22. Y. Abe, S. Lee, E. O. Zayim, C. E. Tracy, J. R. Pitts and S. K. Deb, *Jpn. J. Appl. Phys., Part 1*, **45**, 7780 (2006).
23. A. Avendaño, A. Azens, G. A. Niklasson, and C. G. Granqvist, *Mater. Sci. Eng., B*, **138**, 112 (2007).
24. E. Avendaño, A. Azens, G. A. Niklasson, and C. G. Granqvist, *Sol. Energy Mater. Sol. Cells*, **84**, 337 (2004).